doi.org/10.36721/PJPS. 2023.36.2.REG.483-490.1

A strategy to improve the solubility and bioavailability of the insoluble drug piperlongumine through albumin nanoparticles

Sen Niu[1], Xurui Li[2], Zhongqiu Guo[2], David Wan[3], Yu Liu[2*], Li Li[2], Meng Dong[2] and Xirong Jia[2]

[1]Department of Pharmaceutical Engineering, Xuzhou Pharmaceutical Higher Vocational School of Jiangsu Province, Xuzhou, China
[2]School of Pharmaceutical Sciences, Liaoning University, Shenyang, Liaoning, China
[3]Beijing Rule Biopharma, Co., Ltd., Beijing, China

Abstract: Piperlongumine (PL) is a biologically active alkaloid derived from peppers, has significant cytotoxic effects on cancer with no cytotoxicity. This study used Nab^{TM} technology to prepare PL albumin nanoparticles (PL-BSA-NPs) to improve water solubility and bioavailability. We carried out a pharmacological evaluation of the PL-BSA-NPs. The morphological profile of the PL-BSA-NPs was relatively uniform, with an average particle size of approximately 210 nm, with drug load of 2.1%, and encapsulation rate of 87.6%. PL-BSA-NPs were stable for 4 weeks when stored at 4°C. In vitro release behavior of the PL-BSA-NPs showed a sustained release, with a cumulative release of 67.24% in approximately 24 hours. The pharmacokinetic properties of PL-BSA-NPs were shown that PL-BSA-NPs could maintain a certain level of blood drug concentration for a long time, thus demonstrating the sustained release and increased bioavailability of PL. Finally, we investigated the *in vitro* antitumor activity of the PL-BSA-NPs and found that PL can significantly inhibit HepG2 cell proliferation, and that PL-BSA-NPs enhanced the inhibitory effect of PL on this proliferative effect. Thus, we concluded that PL can destroy liver cancer cells by increasing ROS levels. These results suggested that PL-BSA-NPs show promising potential as a targeted anti-tumor drug.

Keywords: Piperlongumine; albumin nanoparticles; Nab^{TM} technology; pharmacokinetics; antitumor effect

INTRODUCTION

Piperlongumine (PL) or piplartine, 1-[(2E)-3-(3, 4, 5-trimethoxyphenyl) prop-2-enoyl]-1, 2, 5, 6-tetrahydropyridin-2-one. As shown as fig. 1, is a biologically active alkaloid/amide derived from peppers such as the long pepper (*Piper longum* L. -Piperaceae) (Daniel *et al.*, 2013, Lakshmi *et al.*, 2011). It has been found that the anti-inflammatory activity of PL significantly reduced activated microglia and astrocytes in the cortex (Jun *et al.*, 2018). PL can be targeted to, and is selective for a variety of cancer cells (Roh *et al.*, 2014, Liu *et al.*, 2018). PL is freely available and inexpensive and has various pharmacological effects such as analgesia, anti-platelet aggregation, hypolipidemia, anti-fungal, and has been reported to have therapeutic effects against malignant tumors such as hepatocellular carcinoma, breast cancer, gastric cancer, lung cancercolon cancer, liver cancer and glioblastoma (Adams *et al.*, 2012, Jin *et al.*, 2018, Wonhwa *et al.*, 2013, Chen *et al.*, 2015, Bharadwaj *et al.*, 2015, Zhou *et al.*, 2016, Zheng *et al.*, 2016). It has also been shown that PL has potential anticancer activity in cholangiocarcinoma (CCA), and co-exposure of PL with the ROS scavenger N-acetyl-l-cysteine or GSH utterly blocked PL-induced caspase-mediated cell death in CCA cell lines (Thongsom *et al.*, 2017). Furthermore, studied confirmed that time and concentration dependence was the way that PL reduced cell viability and further induced cell apoptosis have and PL had no obvious effect on the distribution of cell cycle (Li *et al.*, 2015). Recent studies have reported that PL's anti-tumor mechanism is related with activation of reactive oxygen stress (ROS) (Colleen *et al.*, 2015). In 2014, Liu prepared polymer micelles by a solid dispersion method, which improved the water solubility and anti-tumor activity of PL. The results indicated that encapsulating PL into biodegradable polymer micelles could enhance its anti-angiogenesis and anti-tumor activity (Liu *et al.*, 2014). Neel *et al.* developed a stable nano emulsion oral administration system for PL, which improved its solubility, oral bioavailability and anti-tumor efficacy (Neel *et al.*, 2016). Furthermore redox-responsive nanoparticles for the stimulus-responsive delivery of PL, were prepared which showed excellent anti-cancer and anti-metastatic effects in the transplanted mouse model (Lee *et al.*, 2018).

Albumin nanoparticles represent a drug delivery system, formed by using albumin as a carrier material for drug embedding. It has a small particle size but a large specific surface area, achieving superior sustained release and targeting, thereby reducing drug toxicity (Danuta *et al.*, 2017). To date, studies have utilized variety of nanoparticles, including micelles, liposomes, emulsions, and micro spheres as drug delivery systems. Amongst these, Protein-based nanoparticles have received extensive concern with their low cytotoxicity, reproducibility, biodegradability, strong drug binding

Corresponding author: e-mail: lnuliuyu@163.com

ability and markedly uptake by target cells (Hasan *et al.*, 2016, Kimura *et al.*, 2018, Si *et al.*, 2018, Ahmed *et al.*, 2012, Mehmet *et al.*, 2020). Saleh *et al.* used curcumin (CCM) as a hydrophobic drug molecule to produce redox-reactive human serum albumin nanoparticles (HAS-NPs) by use of self-assembly HSA molecules (Saleh *et al.*, 2018). Nanoparticle curcumin is different from free CCM, as it is easy to disperse in aqueous medium. Luis used to Bevacizumab-loaded nanoparticles (B-NP) by desolvation. The B-NPs exhibited a markedly higher mean size (310 nm and 180 nm), with a 13% higher payload capacity and lower negative zeta potential (-14 mV and -35 mV) (Luis *et al.*, 2018). Gong published their findings of self-assembled albumin nanoparticles loaded with aclarithromycin A and *in vivo* studies showed that the tumor targeting ability of aclarithromycin A loaded onto albumin nanoparticles in S180 tumor-bearing mice was four times higher than that of the free drug, and its cytotoxicity and cardiotoxicity was lower than that of free aclarithromycin A (Gong *et al.*, 2016). Among the numerous nanoparticles, Bovine serum albumin (BSA) is one of the commonly used model systems to simulate human serum albumin. In the circulatory system, as the main soluble protein, albumin can maintain osmotic pressure and bind and transporting nutrients to the cell (Jianzhong and John, 1999). BSA nanoparticles can be prepared into well-defined sizes, they are biodegradable and have active groups such as amino and carboxyl can bind better with other ligands (Niknejad *et al.*, 2015).

Our previous studies have indicated that PL can bind to albumin spontaneously and that the binding constant (Ka) value was positively related to temperature. In this study, albumin nanoparticles were utilized as a drug carrier to improve the water solubility of PL, thus PL-BSA-NPs were composed as a new drug delivery system to increase bioavailability *in vivo*.

MATERICALS AND METHODS

Materials and reagents

PL and PL reference solution were purchased from Ruishan Co. Ltd. (Shanghai, China). Methylene chloride, anhydrous ethanol, acetone, sodium hydroxide and chromatographic acetonitrile were acquired from Laibo Co. Ltd. (Tianjin, China). Bovine serum albumin (BSA) was supplied from Meilun Co. Ltd. (Dalian, China) and carbamazepine was from Haling Shanghai Co. Ltd. (Shanghai, China). All other chemicals used were of analytical grade.

Synthesis of the PL-BSA-NPs

Firstly, 11 mg of crude PL was accurately weighed and dissolved in a mixing solvent of 3.5mL absolute ethanol and 1mL of dichloromethane. Then the organic phase was prepared by the method described above. Secondly, 0.45g of BSA was dissolved in 36mL of distilled water and adjusted to pH 8 using 0.1mol/L NaOH as the water phase. Thirdly, under high-speed shear (10000 rpm, 15 min), the organic phase was slowly added dropwise to the water phase to make an oil-in-water emulsion. Then, the solution was transferred to a high-pressure micro-jet nanodisperser (80 psi, homogenization 9 times), and rotary evaporated at 50°C to remove the organic solvent, producing an aqueous solution of PL-BSA-NPs. Finally, after lyophilization (addition of 2% sucrose as a lyophilization protective agent), at PL-BSA-NP powder was obtained.

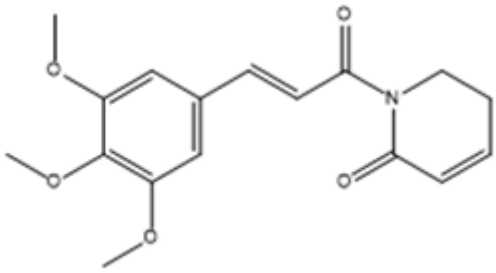

Fig. 1: Chemical structure of piperlongumine.

Characterization

Individual samples such as PL, BSA and PL-BSA-NPs were prepared to a suitable concentration using a UV-Vis spectrophotometer (Yonghua, China) and spectral scanning was performed at the wavelengths ranging from 200 nm to 400 nm. An appropriate amount of PL, PL-BSA-NP freeze-dried powder, BSA and the physical mixture of PL and BSA were placed in separate crucibles, and then measurements by a differential scanning calorimeter (DSC). In the temperature range of 20°C to 400°C, the heating rate adopted is 10°C/min. X-ray diffraction (XRD) analysis was also performed on a D8 X-ray diffractometer from 5°C to 50°C. The size and zeta potential of the PL-BSA-NPs were measured by Malvern zeta sizer (Nano-ZS, Worcestershire, UK) at 25°C. The morphology of PL-BSA-NPs was examined by transmission electron microscopy (TEM). After the solution was dropped on a copper grid and air-dried, it was observed with JEM-2100 transmission electron microscope (JEOL, Japan).

Determination of drug loading and encapsulation yields

The drug loading and encapsulation efficiency of the PL-BSA-NPs were determined by HPLC (Agilent 1200 HPLC, Worcestershire, UK). The PL-BSA-NP solution was centrifuge at 4°C (10000 rpm, 30 min) and the supernatant was removed and used to determine the free drug content. And the encapsulation efficiency (EE) was calculated as follow:

$$EE(\%) = \frac{Total\ amount\ of\ PL - Free\ PL}{Total\ amount\ of\ PL} \times 100\%$$

An aliquot of the lyophilized PL-BSA-NPs was dissolved in distilled water and methanol was added to demulsify the solution. Then the drug loading (DL) for PL was calculated using the following equation:

$$DL(\%) = \frac{Total\ amount\ of\ PL - Free\ PL}{Total\ amount\ of\ PL - BSA - NPs} \times 100\%$$

Stability experiments

The samples of lyophilized PL-BSA-NPs were stored at 4°C. And the samples were used periodically for analysis. Changes in size and encapsulation yields, (if any), were also monitored.

Evaluation of drug release from the PL-BSA-NPs

PL-BSA-NPs (2mL) were processed using a dialysis bag, and then resuspended into PBS pH 7.4 at 37°C for 48 h to demonstrate the drug release profiles. At predetermined interval (0.5h, 1h, 2h, 3h, 4h, 6h, 8h, 12h, 24h, 36h and 48 h), 1mL of each sample was removed. To maintain the total volume, add the same volume of isothermal buffer. The concentration of the released PL-BSA-NPs was measured with a UV/visible spectrophotometer.

Hemolysis experiment of PL-BSA-NPs

Before the pharmacokinetic study, the hemolysis experiment was carried out first. We got full blood from the Sprague-Dawley (SD) rats and collected it in an EDTA anticoagulant tube, 3000r/min centrifuged 15min to obtain blood cells. Prepared 1mL ultra-pure water, 1mL PBS solution and 1mL of PL-BSA-NPs with different concentrations (10-100μg/mL), respectively mixed with 20μL of blood cells. After incubation at 37°C for 4h, then centrifuged 15min at 3000r/min. Finally, the hemolytic phenomenon can be observed.

Pharmacokinetic study in rats

The pharmacokinetics of PL-BSA-NPs were evaluated in Sprague-Dawley (SD) rats. All animal studies were approved by the University Ethics Committee and in accordance with the Principles of Laboratory Animal Care. SD rats (males, 250±20g) were randomly divided into two groups and PL-BSA-NPs and PL solutions were administered intravenously at a single dose of 50mg/kg PL through the tail vein. Bloods were collected from rats orbit (approximately 500μL) at 5min, 10min, 30min, 1h, 2h, 4h, 8h and 12h. Placed the blood samples into heparinized tubes and then centrifuged at 4000 rpm for 10 min (4°C). The supernatants containing the plasma samples were stored at -80ºC until use.

In vitro cytotoxicity test

To examine the anticancer activities of the albumin nanoparticles, the cytotoxicity of the PL-BSA-NPs and PL solutions were tested using HepG2 cells and a conventional MTT assay was conducted. Briefly, HepG2 cells (5.0*103) were seeded into each well of a 96-well plate and then incubated for 24h to allow cell attachment. Then, the cells were incubated with the PL-BSA-NPs and PL solution (final concentrations of PL were 5, 7.5, 10, 15 and 20μmol/L) for 24h. Thereafter, the cells were incubated for 24h and 100μL of MTT solution (5mg/mL) and 100μL of DMSO were added to the wells. The absorbance was then measured at 570nm with a multimode micro plate reader, the block cells were taken as control group. Then the relative cell viability (%) was calculated as (absorbance of the test group/absorbance of the control group) *100.

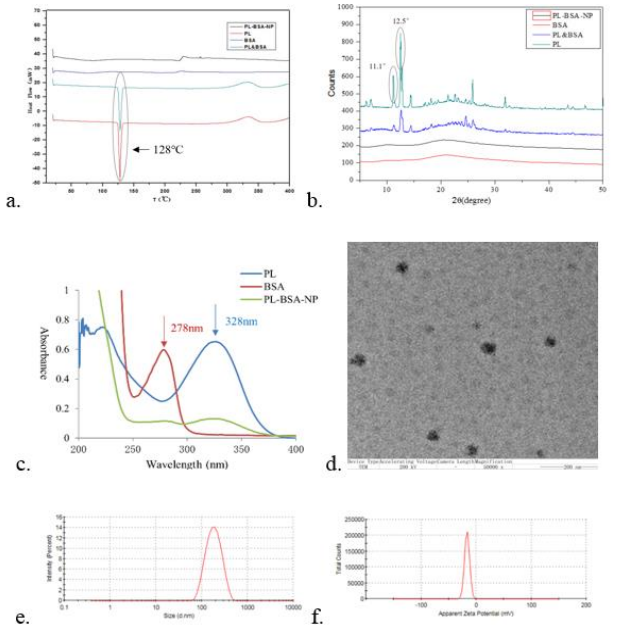

Fig. 2(a): DSC of PL, BSA, PL&BSA and PL-BSA-NPs, (b) XRD of PL, BSA, PL&BSA and the PL-BSA-NPs, (c)UV spectrum of PL, BSA and PL-BSA-NPs, (d). TEM of the PL-BSA-NPs, (e) Particle size distribution of the PL-BSA-NPs, (f) Zeta potential of the PL-BSA-NPs.

Quantification of intracellular ROS

A fluorescent probe 2'-7'-dichlorofluorescein diacetate (DCFH-DA, Sigma-Aldrich, Germany) was used to evaluate the accumulation of intracellular reactive oxygen species (ROS) by flow cytometry. First, HepG2 cell line (5*103/mL) was seeded into 6-well plates for 24 hours, and cells were treated with different concentrations of PL-BSA-NPs and PL solutions (5, 10 and 20μmol/mL) for 24 hours. Secondly, after washing HepG2 cells with PBS, they were incubated with 100μL of DCFH-DA for 30 min at 37°C in a humidified 5% CO_2 incubator. Finally, DCFH-DA was removed and cells were washed with PBS, trypsinized and resuspended in complete medium, and fluorescence intensity was measured at 488 nm by flow cytometry.

STATISTICAL ANALYSIS

Each experiment and measurement were performed independently no less than triplicates. All data in this study are expressed as mean ± standard deviation (SD). The P value was statistically analyzed with one sample t test in a basic model of SPSS 19.0. A P value of <0.05 was considered statistically significant.

RESULTS

Characterization of DSC of PL-BSA-NPs

To determine the state of PL in albumin nanoparticles, DSC was performed for PL, BSA, blank PL-BSA (PL&BSA) and the PL-BSA-NPs and the thermal analysis of DSC is exhibited in fig. 2 (a). BSA and the PL-BSA-NPs showed smooth DSC curves in the temperature range of 0-400°C. The DSC graphs for PL and PL&BSA both had a sharp melting point peak near 128°C, which is consistent with the thermal behavior of PL (Vaishali *et al*., 2022).

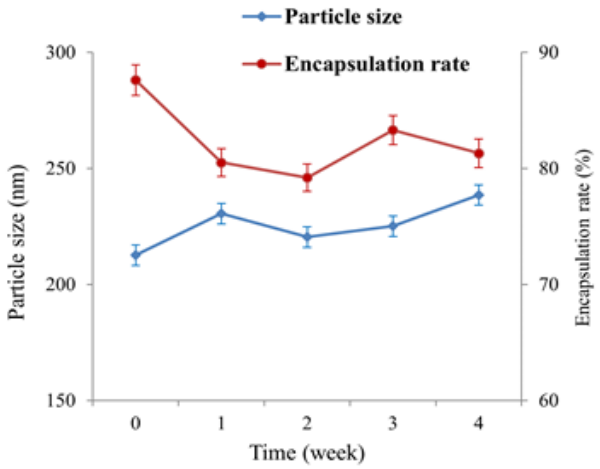

Fig. 3: Stability of the PL-BSA-NPs.

Characterization of XRD of PL-BSA-NPs

The crystalline phases of PL, BSA, PL&BSA and PL-BSA-NPs were analyzed by XRD analysis. X-ray diffraction is one of the commonly used qualitative methods, used to analyze the data derived from the dispersion and physical state of a drug and the polymer matrix. As is demonstrated in fig. 2 (b), the diffractogram for pure PL and PL&BSA exhibited an intense peak at 2θ equal to 11.1◦ and 11.25◦ owing to their high crystalline structure (Krunal *et al.*, 2022). Nevertheless, When PL was in NPs, no obvious PL characteristic peaks can be examined.

Characterization of UV–Vis of PL-BSA-NPs

The synthesis of the PL-BSA-NPs was also confirmed using UV-Vis comparison. The UV-Vis absorption spectra of native PL, BSA and PL-BSA-NPs are shown in fig. 2 (c). The wavelength range of the UV-Vis spectrum is between 200 and 400 nm and the absorption around 220 nm and 328 nm represented PL with a peak wavelength of BSA at 278 nm; it's the characteristic peak of protein in BSA (Xingjia *et al.*, 2009).

Morphological observation of PL-BSA-NPs

The morphology of the surface of the PL-BSA-NPs was analyzed by TEM which clearly showed their pore sizes and also showed small and homogeneous particles of approximately 200 nm, appearing as clear single spherical shapes with no clumping (fig. 2 (d)).

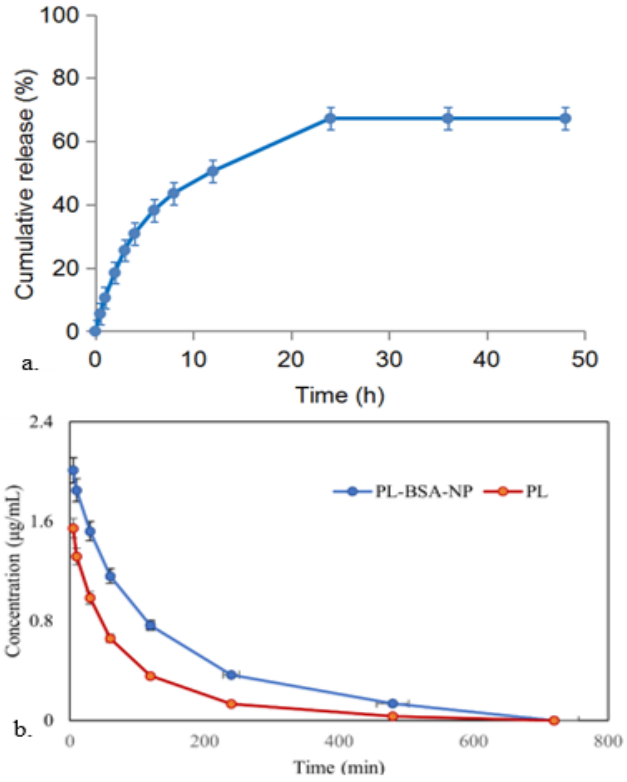

Fig. 4: (a) *In vitro* release curve for the PL-BSA-NPs, (b) Plasma concentration and time curve for PL and the PL-BSA-NPs.

Particle size and zeta potential of PL-BSA-NPs

The average particle size of the PL-BSA-NPs was 210.3 nm (fig. 2 (e)), which was consistent with the TEM data. This indicated the successful synthesis of nanoscale dispersed nanoparticles. The zeta potential analysis confirmed the formation of polyelectrolytes (Zeta potential -16.7 mV, fig. 2 (f)). The absolute value of the zeta potential of PL-BSA-NP was higher than 15 mV.

Stability studies of PL-BSA-NPs

The stability of a drug-carrier complex is critical for a drug delivery system (Jonathan *et al.*, 2012). Therefore, the stability of the PL-BSA-NPs was assessed and the results are shown in fig. 3. PL-BSA-NPs were found to be stable in normal saline for 4 weeks with no aggregation of the particles and the particle size was always in the range of 210-240nm and the encapsulation efficiency were always higher than 80%. The encapsulation efficiency (EE%) and the drug loading (DL%) of PL-BSA-NPs was 87.6% and 2.1% when the nanoparticles were freshly prepared. It's similar to the stability described in the literature (Aodah *et al.*, 2016). It may be because PL and BSA are connected by hydrogen bonds and van der Waals interactions (Nayara *et al.*, 2019, Rose and Subramanian, 1981).

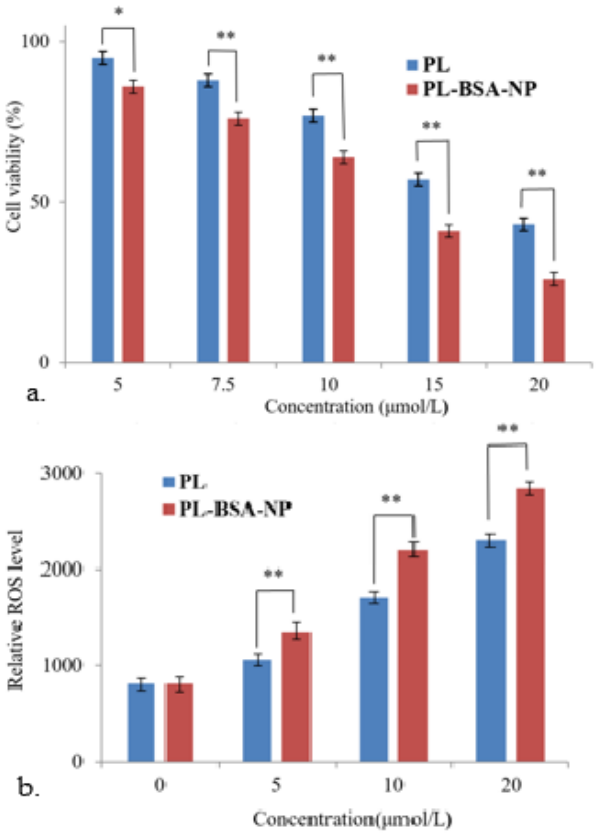

Fig. 5: (a). Effect of PL and the PL-BSA-NPs on HepG2 Cell viability, (b) Effects of PL and the PL-BSA-NPs on ROS levels in HepG2 cells (**P<0.05*; ***P<0.01*).

In vitro drug release study

The drug release studies for the PL-BSA-NPs were implemented at pH 7.4 (physiological pH) and the results are shown in fig. 4 (a). A rush release was found in the first 4h followed by a controlled release of PL over a period of 24h. The surface adsorbed PL was released initially from the surface of the nanoparticles in the first 4h, causing the release of 31.25% of total PL. The results revealed that almost 67.24% of the drug was released within the next 24h at physiological tumor pH and the drug was released stably from 24 to 48 hours. As shown in fig. 4 (a), the drug maintained a stable release after 24 h.

Hemolytic experiment of PL-BSA-NPs

In the hemolytic experiment, the ultra-pure water group was a positive control group, the PBS group was a negative control group, and the PL-BSA-NPs of each concentration was used as the experimental group. After centrifugal observation, it was found that the ultra-pure water group was red, indicated that the phenomenon of hemolysis occurred. The PBS group and the PL-BSA-NPs group sinking into the bottom of the pipe, the solution was clear and transparent, indicated that no hemolytic phenomenon occurred. Therefore, according to the hemolytic examination standards, the PL-BSA-NPS group did not occur hemolysis. (Shiqi *et al.*, 2021).

Pharmacokinetic studies in vivo

In order to confirm whether the PL-BSA-NPs drug delivery system has improved bioavailability, the pharmacokinetics in rats were evaluated with PL as the control group. The plasma concentration-time profiles of the PL and the PL-BSA-NPs are shown in fig. 4 (b). The pharmacokinetic parameters are displayed in table 1. The pharmacokinetic parameters were obtained by using DAS 2.0 pharmacokinetic data analysis software and the principle of statistical moments to analyze the blood concentration-time curve of the PL-BSA-NPs and PL by non-compartment model analysis. It can be clearly seen that the PL group and the PL-BSA-NPs group are significantly different from each other in parameters. Compared to rats treated with PL, rats treated with the PL-BSA-NPs showed higher drug concentrations at all time points. Consequently, the terminal elimination half-life ($T_{1/2}$) was prolonged for the PL-BSA-NPs over PL alone (141.34±4.37 vs 69.13±5.28 min). The $T_{1/2}$ for the PL-BSA-NPs was over two times that of PL. The mean residence time ($MRT_{0-\infty}$) for PL was 93.94±2.41 min and the $MRT_{0-\infty}$ for the PL-BSA-NPs was 151.75±3.25. The $MRT_{0-\infty}$ for the PL-BSA-NPs was about twice as long as PL alone. The conclusions derived from the $MRT_{0-\infty}$ data are consistent with the conclusions for $T_{1/2}$. Furthermore, the systemic clearance (CL) was significantly reduced for the PL-BSA-NPs when compared to PL (0.14±0.07 vs 0.26±0.11 L/min/kg) and the CL of the PL-BSA-NPs was approximately half that of PL. In the PL group virtually, no drug was detected in their plasma at about 8 hours. However, there was still drug present in the plasma of rats from the PL-BSA-NPs group, and the drug stayed *in vivo* for longer. The area under curve ($AUC_{0-\infty}$) for PL and the PL-BSA-NPs were 168.79±21.42 and 372.31±18.36 mg/mL*min, respectively. When compared to the AUC for the PL-BSA-NPs, the value was more than double that seen for PL and this higher AUC indicated a significant increase *in vivo* bioavailability.

In vitro cell cytotoxicity test

Next cell viability was determined using the MTT assay to characterize cell growth inhibition caused by PL and the PL-BSA-NPs using a human hepatocellular carcinoma cell line (HepG2 cell). HepG2 cells were exposed to different concentrations for 24h and cellular morphological changes were observed and this can be seen in the histogram from fig. 5 (a). Here, the ability of PL and PL-BSA-NPs to inhibit cell proliferation increased with increasing dose. The concentration of PL was proportional to proliferation inhibition in these cells. As the concentration of PL increased, the inhibitory effect on HepG2 cells became stronger. In addition, when the concentration of PL reached 20μmol/L, the cell survival rate of the PL group was 43.21% and that of the PL-BSA-NPs group was 26.18%. The half maximal inhibitory concentration (IC_{50}) of the PL-BSA-NPs was found to be approximately 12.62 μmol/L while that of PL alone was 17.31 μmol/L.

Table 1: Pharmacokinetic parameters of PL and the PL-BSA-NPs (n=4) (Comparison between PL and the PL-BSA-NPs, *P<0.05; **P<0.01.)

Parameters	PL	PL-BSA-NPs
$T_{1/2}$ (min)	69.13±5.28	141.34±4.37**
AUC_{0-t} (mg/L*min)	168.63±13.46	364.82±26.14**
$AUC_{0-\infty}$ (mg/L*min)	168.79±21.42	372.31±18.36**
CL (L/min/kg)	0.26±0.11	0.14±0.07*
$MRT_{0-\infty}$ (min)	93.94±2.41	151.75±3.25**

Determination of cell ROS accumulation

The effects of PL and PL-BSA-NPs on cellular ROS levels were determined by flow cytometry and a redox-sensitive fluorescent probe DCFH-DA. It can be observed in fig. 5 (b) that after 24 hours of treatment with different concentrations of PL and PL-BSA-NPs, the increased level of ROS in cancer cells was proportional to the dose. In addition, compared with PL, PL-BSA-NPs had higher ROS levels due to enhanced tumor uptake ($p<0.05$).

DISCUSSION

Characterization of PL-BSA-NPs

The characteristic peak of PL did not appear in the DSC analysis of the PL-BSA-NPs, but in the physical mixture of PL&BSA and blank PL, which indicated that PL is encapsulated in albumin NPs. The conclusion can be further verified by the characterization of UV-Vis and XRD. The X-ray diffraction pattern observed for PL-BSA-NPs is corroborated. The characteristic peaks of PL still remain in the PL&BSA diffractogram, indicating that the crystal form of PL does not change after physical mixing. However, in the diffraction pattern of PL-BSA-NPs, the characteristic peaks of PL disappeared, indicating that the crystal form of PL in PL-BSA-NPs was changed, and it was encapsulated in BSA in an amorphous or disordered state. The results of DSC, UV-Vis and XRD all confirmed that PL was encapsulated into the nanoparticles and existed in an amorphous structure. This indicated that the drug can be continuously released from the nanoparticles and its bioavailability can be improved (Saleh *et al.*, 2018). The morphological observation was attributed to the good dispersion of the nanoparticles and the uniform particle size. The particle size and zeta potential indicating that the more stable the system was, it could resist aggregation after dispersion and had good dispersion (Ali et al., 2011).

Stability studies of PL-BSA-NPs

By the stability studies, we can conclude that no obvious alteration in the encapsulation efficiency or the drug loading was seen, indicating good stability of the PL-BSA-NPs. It demonstrated that PL-BSA-NPs can be stored stably for a long time and its properties basically do not change.

In vitro and in vivo drug release study

The results confirmed that the PL-BSA-NPs have a sustained release effect. The release profile of PL-BSA-NPs indicated its potential applicability as a drug delivery system, with the advantages of significantly prolonged release time in vivo, better sustained release effect and significantly increased drug release amount. The Pharmacokinetic results indicated that the PL-BSA-NPs was eliminated in vivo more slowly than PL alone and improved the bioavailability of drugs in vivo.

In vitro cell test

The cell viability experiment showed that the PL-BSA-NPs were more effective at inhibiting cell growth when compared to PL after a 24 h incubation time, and present a clear concentration dependence. We preliminarily inferred that PL-BSA-NPs could kill liver cancer cells by inducing an increase in the level of intracellular ROS. PL can improve the level of ROS in the tumor cells and further induce the death of tumor cells (Lakshmi et al., 2011). Therefore, we infer that the changes in cytotoxicity are related to the fluctuations of ROS levels (Hong et al., 2018).

CONCLUSION

In this study, we successfully synthesized a novel drug delivery system PL-BSA-NPs using Nab TM. To improve the water solubility and in vivo bioavailability of PL, albumin was selected as the drug carrier. The results showed that the structure of the synthesized PL-BSA-NPs represented a relatively uniform spherical shape, with an average particle size of approximately 210nm, a drug loading of 2.1% and an encapsulation efficiency of 87.6%. Within the PL-BSA-NPs, the crystalline structure of PL changed and existed in an amorphous state and was encapsulated in albumin molecules. When the PL-BSA-NPs were stored at 4°C they remained stable at 4 weeks. Furthermore, the PL-BSA-NPs possessed a sustained release in vivo and enhanced the inhibitory effect of PL on tumor cell proliferation. When compared to PL, the PL-BSA-NPs produced a higher ROS level due to the enhanced tumor uptake.

Thus, our preliminarily study suggests that PL can destroy liver cancer cells by inducing an increase in intracellular ROS levels. Taken together, the biocompatible of the PL-BSA-NPs is suitable for these nanoparticles to be used as an antitumor drug with high potential in a variety of applications, including chemotherapy.

ACKNOWLEDGMENTS

This work was supported by the LiaoNing Revitalization Talents Program of China (grant number XLYC2007054) and the Department of Education of Liaoning Province (grant number LJKZ0095).

CONFLICT OF INTERNET

The authors declare that they have no conflict of interest.

HUMAN AND ANIMAL SUBJECTS

The authors declare that no experiments were performed on humans. All studies of animal experiments were approved by the Institutional Animal Care, and conducted in accordance with the guidelines of the Committee on the Care and Use of Laboratory Animals in China.

REFERENCES

Adams DJ, Dai M, Pellegrino G, Wagner BK, Stern AM, Shamji AF and Schreiber SL (2012). Synthesis, cellular evaluation, and mechanism of action of piperlongumine analogs. *PNAS*, **109**(38): 15115-20.

Ahmed OE, Wael MS and Nazik AE (2012). Albumin-based nanoparticles as potential controlled release drug delivery systems. *J. Control Release*, **157**(2): 168-182.

Ali D, Ahmad M, Rasoul S, Mohammad HF, Zahra G and Alma. UD (2011). Bioactive glass nanoparticles with negative zeta potential. *Ceram Int*, **37**(7): 2311-2316.

Aodah A, Pavlik A, Karlage K and Myrdal PB (2016). Preformulation sudies on pperlongumine. *PLoS One.*, **11**(3): e0151707.

Bharadwaj U, Eckols TK, Kolosov M, Kasembeli MM, Adam A, Torres D, Zhang X, Dobrolecki LE, Wei W, Lewis MT, Dave B, Chang JC, Landis MD, Creighton CJ, Mancini MA and Tweardy DJ (2015). Drug-repositioning screening identified piperlongumine as a direct STAT3 inhibitor with potent activity against breast cancer. *Oncogene*, **34**(11): 1341-53.

Chen Y, Liu JM, Xiong XX, Qiu XY, Pan F, Liu D, Lan SJ, Jin S, Yu SB and Chen XQ (2015). Piperlongumine selectively kills hepatocellular carcinoma cells and preferentially inhibits their invasion via ROS-ER-MAPKs-CHOP. *Oncotarget.*, **6**(8): 6406-6421.

Colleen RR, Navdeep SC (2015). ROS-dependent signal transduction. *Curr Opin Cell Biol*, **33**: 8-13.

Daniel PB, Claudia P, Manoel OM, Nicolau SN, Edilberto RS and Leticia VCL (2013). Overview of the therapeutic potential of piplartine (piperlongumine). *Eur J Pharm Sci*, **48**(3): 453-463.

Danuta P, Małgorzata MJ and Zygmunt HZ (2017). The role of nanoparticles in the albumin-cytarabine and albumin-methotrexate interactions. *Mat Sci Eng C*, **73**: 388-397.

Gong G, Liu W and Wang S (2016). Self-assembled albumin nanoparticles as a nanocarrier for aclacinomycin A. *Nanotechnology*, **27**(46): 465602.

Hasan K and Seyed AS (2016). Protein-based nanoparticles as a nanobiotechnological tool for cancer theranostics. *New Biotechnology*, **33**: S148.

Hong EJ, Lee DY, Kang HC, Kim YC and Shim MS (2018). Cancer-specific pro-oxidant therapy using low toxic polypeptide micelles encapsulating piperlongumine. *J Ind Eng Chem*, S1226086X18300571.

Jianzhong W and John MP (1999). Osmotic pressures of aqueous bovine serum albumin solutions at high ionic strength. *Fluid Phase Equilibria*, **155**(1): 139-154.

Jin SS, Chang HJ, Michael CP, Han GS, Hyunjin Y, Kwonho H and Sung GH (2018). Piperlongumine decreases cell proliferation and the expression of cell cycle-associated proteins by inhibiting Akt pathway in human lung cancer cells. *Food Chem Toxicol*, **111**: 9-18.

Jonathan RD, Adam C, Tara C, Brian B, Habib S, Riccardo P and Kevin S (2012). A versatile polymer micelle drug delivery system for encapsulation and in vivo stabilization of hydrophobic anticancer drugs. *J Drug Deliv*, **2012**: 8.

Jun G, Thi-Kim-Quy H, Ji YS, Tae-Shin P, Young-Kyoung R, Hye-Yeon P, Jung-Ran N, Yong-Hoon K, Jung HH, Dong-Hee C, Dae YH, Sanghee K, Chul-Ho L, Won KO and Kyoung-Shim K (2018). Piperlongumine activates Sirtuin1 and improves cognitive function in a murine model of Alzheimer's disease. *J Funct Foods*, **43**: 103-111.

Kimura K, Yamasaki K, Nakamura H, Haratake M, Taguchi K and Otagiri M (2018). Preparation and in vitro analysis of human serum albumin nanoparticles loaded with anthracycline derivatives. *Chem. Pharm. Bull.*, **66**(4): 382-390.

Krunal P, Poonam J, Pradeep KR, Ashok KJ, Raghu S, Hitesh K and Sunita P (2022). Human serum albumin-based propulsive Piperlongumine-loaded nanoparticles: Formulation development, characterization and anti-cancer study. *Colloid Surface A*, **652**: 129738.

Lakshmi R, Takao I, Aditi UG, Michael F, Monica S, Xiaoyu L, Nicola JT, Todd RG, Steven AC, Alykhan FS, Andrew MS, Anna M, Stuart LS and Sam WL (2011). Selective killing of cancer cells by a small molecule targeting the stress response to ROS. *Nature*, **475**(7355): 231-234.

Lee HL, Hwang SC, Nah JW, Kim J, Cha B, Kang DH and Jeong YI (2018). Redox and pH-responsive nanoparticles release piperlongumine in a stimuli-sensitive manner to inhibit pulmonary metastasis of colorectal carcinoma cells. *J. Pharm Sci.*, **107**(10): 2702-2712.

Li W, Wen C, Bai H, Wang X, Zhang X, Huang L, Yang X, Iwamoto A and Liu H (2015). JNK signaling pathway is involved in piperlongumine-mediated apoptosis in human colorectal cancer HCT116 cells. *Oncology letters*, **10**(2): 709-715.

Liu Y, Chang Y, Yang C, Sang Z, Yang T, Ang W, Ye W,

Wei Y, Gong C and Luo Y (2014). Biodegradable nanoassemblies of piperlongumine display enhanced anti-angiogenesis and anti-tumor activities. *Nanoscale.*, **6**(8): 4325-37.

Liu Y, Li QY, Wang YP, Liu YM, Liu B, Liu MM and Liu BM (2018). Spectroscopic investigation of the anticancer alkaloid piperlongumine binding to human serum albumin from the viewpoint of drug delivery. *Luminescence*, **33**(2): 305-311.

Luis RI, Boiero C, Martínez-Ohárriz MC, Agüeros M, Ramos R, Penelas I, Allemandi D, Llabot JM and Irache JM (2018). Human serum albumin nanoparticles for ocular delivery of bevacizumab. *Int. J. Pharm*, **541**(1-2): 214-223.

Mehmet EO, Ioannis DK, Zeynep S, Neslihan UO and Panoraia IS (2020). Recent trends on wound management: New therapeutic choices based on polymeric carriers. *Asian J Pharm Sci*, **15**(6): 661-684.

Nayara SAC, Ícaro Putinhon C, Daniel PB, Jose MBF and Marinonio LC (2019). An investigation into the interaction between piplartine (piperlongumine) and human serum albumin. *Spectrochim Acta A Mol. Biomol. Spectrosc.*, **220**: 117084.

Neel MF, Hussaini SSQ, Xinli L and Sanjay KS (2016). Nanoemulsion formulations for anti-cancer agent piplartine-Characterization, toxicological, pharmaco-kinetics and efficacy studies. *Int. J. Pharm*, **498**(1-2): 12-22.

Niknejad H and Mahmoudzadeh R (2015). Comparison of different crosslinking methods for preparation of docetaxel-loaded albumin nanoparticles. *Iran. J. Pharm. Res*, **14**(2): 385-394.

Roh JL, Kim EH, Park JY, Kim JW, Kwon M and Lee BH (2014). Piperlongumine selectively kills cancer cells and increases cisplatin antitumor activity in head and neck cancer. *Oncotarget.*, **5**(19): 9227-9238.

Ross PD and Subramanian S (1981). Thermodynamics of protein association reactions: Forces contributing to stability. *Biochemistry*, **20**(11): 3096-102.

Saleh T, Soudi T and Shojaosadati SA (2018). Redox responsive curcumin-loaded human serum albumin nanoparticles: Preparation, characterization and *in vitro* evaluation. *Int. J. Biol. Macromol.*, **114**: 759-766.

Si S, Qian-Ru X, Yang W and Yong J (2018). Roles of alcohol desolvating agents on the size control of bovine serum albumin nanoparticles in drug delivery system. *J Drug Deliv Sci Tec*, **47**: 193-199.

Shiqi G, Yanan S, Yanzi L, Lanze L, Kaoxiang S and Youxin L (2021). Relationship and improvement strategies between drug nanocarrier characteristics and hemocompatibility: What can we learn from the literature. *Asian J Pharm Sci*, **16**(5): 551-576.

Thongsom S, Suginta W, Lee KJ, Choe H and Talabnin C (2017). Piperlongumine induces G2/M phase arrest and apoptosis in cholangiocarcinoma cells through the ROS-JNK-ERK signaling pathway. *Apoptosis*, **22**(11): 1473-1484.

Vaishali Y, Anuja K, Mirza SB, Muhammed M, Mahadeva N and Divya V (2022). Decrypting the interaction pattern of Piperlongumine with calf thymus DNA and dodecamer d(CGCGAATTCGCG)(2) B-DNA: Biophysical and molecular docking analysis. *Biophys Chem*, **285**: 106808.

Wonhwa L, Hayoung Y, Jeong AK, Sangkyu L, Jun-Goo J, Min YL, You-Mie L and Jong-Sup B (2013). Barrier protective effects of piperlonguminine in LPS-induced inflammation *in vitro* and *in vivo*. *Food Chem Toxicol*, **58**: 149-157.

Xingjia G, Lei Z, Xiudan S, Xiaowei H, Chuang G and Pingli K (2009). Spectroscopic studies on the interaction between sodium ozagrel and bovine serum albumin. *J. Mol. Struct*, **928**(1-3): 114-120.

Zhou L, Liang X, Zhang L, Yang L, Nagao N, Wu H, Liu C, Lin S, Cai G and Liu J (2016). MiR-27a-3p functions as an oncogene in gastric cancer by targeting BTG2. *Oncotarget.*, **7**(32): 51943-51954.

Zheng J, Son DJ, Gu SM, Woo JR, Ham YW, Lee HP, Kim WJ, Jung JK and Hong JT (2016). Piperlongumine inhibits lung tumor growth via inhibition of nuclear factor kappa B signaling pathway. *Sci Rep.*, **6**: 26357.